

Multiband theory of multi-exciton complexes in self-assembled quantum dots

Weidong Sheng,* Shun-Jen Cheng,[†] and Pawel Hawrylak

Institute for Microstructural Sciences, National Research Council of Canada, Ottawa ON K1A 0R6, Canada

(Received 16 February 2004; revised manuscript received 27 August 2004; published 13 January 2005)

We report on a multiband microscopic theory of many-exciton complexes in self-assembled quantum dots. The single particle states are obtained by three methods: single-band effective-mass approximation, the multiband $\mathbf{k}\cdot\mathbf{p}$ method, and the tight-binding method. The electronic structure calculations are coupled with strain calculations via Bir-Pikus Hamiltonian. The many-body wave functions of N electrons and N valence holes are expanded in the basis of Slater determinants. The Coulomb matrix elements are evaluated using statically screened interaction for the three different sets of single particle states and the correlated N -exciton states are obtained by the configuration interaction method. The theory is applied to the excitonic recombination spectrum in InAs/GaAs self-assembled quantum dots. The results of the single-band effective-mass approximation are successfully compared with those obtained by using the of $\mathbf{k}\cdot\mathbf{p}$ and tight-binding methods.

DOI: 10.1103/PhysRevB.71.035316

PACS number(s): 73.21.La, 78.67.Hc, 71.15.-m, 71.35.Cc

I. INTRODUCTION

Semiconductor self-assembled quantum dots (SAQDs)¹⁻³ are islands of one semiconductor, e.g., InAs, in a host matrix of another semiconductor, e.g., GaAs. The elementary excitations, electrons and holes, are believed to be confined in all three dimensions by the band gap difference between island and matrix materials. The picture of electrons and holes as confined elementary excitations with effective mass, interacting via Coulomb interactions has been successfully applied toward the explanation of many experimental results.⁴⁻¹¹ It is important to establish to what extent the effective-mass picture is applicable to the description of electronic states of self-assembled quantum dots by a systematic comparison of different approaches. The self-assembled quantum dots plus the surrounding barrier material contain millions of atoms and the density functional *ab initio* calculations are not possible yet. Hence, in this work we compare two approaches, the multiband $\mathbf{k}\cdot\mathbf{p}$ method and the tight-binding method with the predictions of the effective-mass calculations. The multiband $\mathbf{k}\cdot\mathbf{p}$ method¹²⁻¹⁸ accounts for the proper structure of the valence band, including heavy, light, and spin split-off hole bands. It is, however, limited to the top of the valence band, does not account for the atomistic character of the interfaces between the dot and barrier material, and is expected to break down as the size of the nanostructure decreases. The atomistic structure of the nanostructure is captured in either the tight-binding^{19,20} or pseudopotential approaches as developed by Zunger and co-workers.²¹ The tight-binding approach chosen here is the effective bond orbital model (EBOM),²²⁻²⁴ a version of sp^3 tight-binding models. The advantage of EBOM is that it extrapolates to the $\mathbf{k}\cdot\mathbf{p}$ approach making a direct comparison possible. The disadvantage of EBOM is that it misses the lack of inversion symmetry of zinc blende structures.

The single particle energy levels are not measured directly. What is measured in, e.g., optical experiments, is the emission from self-assembled quantum dots as a function of the excitation power, or the number of electrons and holes in the dot. The electrons and holes interact and form multiexciton complexes. Emission from multiexciton complexes has

been measured by a number of groups.^{6-9,25-30} The higher the pumping intensity is, the more excitons are involved, thus the emission from higher excited electron and hole states can be observed. The multiexciton emission spectra have been interpreted using quantum mechanical methods such as the Hartree-Fock method and the configuration interaction method (CI),³¹ in which the multiexciton complex states are constructed from single-particle states of the system. It is a challenge to combine realistic single-particle states calculated for the million-atom structures with these quantum mechanical methods. A number of theoretical approaches have been proposed to address this issue, such as combining multiband $\mathbf{k}\cdot\mathbf{p}$ single-particle states with self-consistent Hartree-Fock method¹⁶ and combining single-band effective-mass^{9,32-35} or microscopic pseudopotential wave functions with CI.^{36,37}

In this paper, we use a general approach which combines different multiband calculations of single-particle states with the CI method for the calculation of multi-exciton states. By using single-particle states obtained from the single-band effective-mass approximation, the multiband $\mathbf{k}\cdot\mathbf{p}$ method and the atomistic tight-binding-like method, we are able to compare the multiexciton emission spectra obtained from different single-particle states and determine both the validity of the effective-mass approximation as well as the validity of multiexciton emission spectra as fingerprints of electronic structure of quantum dots.

II. SINGLE-PARTICLE CALCULATION

The single particle calculations for self-assembled quantum dots started with the effective-mass calculations which related shape and size of the dots to the single particle energy levels.³⁸ As experimental information accumulated, more sophisticated approaches were developed, such as single-band effective-mass method coupled with strain calculation,³⁹⁻⁴¹ eight-band $\mathbf{k}\cdot\mathbf{p}$ method,¹⁴⁻¹⁷ tight-binding methods,^{20,23} and the empirical pseudopotential method.²¹ In the following, we briefly describe the single-band effective-mass method, the eight-band $\mathbf{k}\cdot\mathbf{p}$ method and EBOM for the calculation of single-particle states in SAQDs.

A. Effective-mass single-particle states

Here we use a single-band model with anisotropic effective masses of electrons and holes. The goal is to verify whether one can obtain the correct energy spectrum of levels in SAQDs⁴⁸ by this relatively simple method. As the effective masses are known to be very different in SAQDs from those in bulk materials,⁵ they are treated as adjustable parameters that can be obtained either from experiments or from more sophisticated methods like the multiband $\mathbf{k}\cdot\mathbf{p}$ and the tight-binding methods.

The Hamiltonians, including strain, read

$$\hat{H}_e = -\frac{\hbar^2}{2m_{\parallel}^e} \left(\frac{\partial^2}{\partial x^2} + \frac{\partial^2}{\partial y^2} \right) - \frac{\hbar^2}{2m_{\perp}^e} \frac{\partial^2}{\partial z^2} + a_c H_s + V_{bo}^e + V_P,$$

$$\hat{H}_h = \frac{\hbar^2}{2m_{\parallel}^h} \left(\frac{\partial^2}{\partial x^2} + \frac{\partial^2}{\partial y^2} \right) + \frac{\hbar^2}{2m_{\perp}^h} \frac{\partial^2}{\partial z^2} - a_v H_s - b B_s + V_{bo}^h - V_P, \quad (1)$$

where $H_s = \varepsilon_{xx} + \varepsilon_{yy} + \varepsilon_{zz}$ and $B_s = \varepsilon_{zz} - 1/2(\varepsilon_{xx} + \varepsilon_{yy})$ is the hydrostatic and biaxial strain component, respectively, V_{bo}^e and V_{bo}^h are the potentials from the band offsets between island (InAs) and matrix (GaAs) material, and V_P is the piezoelectric potential.¹⁶ a_c , a_v , and b are the deformation potential parameters that are also used in the multiband $\mathbf{k}\cdot\mathbf{p}$ method and EBOM.

B. Eight-band $\mathbf{k}\cdot\mathbf{p}$ single-particle states

The eight-band $\mathbf{k}\cdot\mathbf{p}$ method uses eight Bloch functions at the Γ point of the Brillouin zone as basis functions to describe electron states with finite wave vector. As the lateral size of SAQDs is usually much larger than the lattice constant, it has been widely used in the calculation of confined electron states in SAQDs.¹³⁻¹⁵ In general, the multiband $\mathbf{k}\cdot\mathbf{p}$ Hamiltonian can be written as

$$\hat{H}_{\mathbf{k}\cdot\mathbf{p}} = \mathbf{E}_{bo} + \mathbf{A}_x \hat{k}_x \hat{k}_x + \mathbf{A}_y \hat{k}_y \hat{k}_y + \mathbf{A}_z \hat{k}_z \hat{k}_z + \mathbf{B}_{xy} \hat{k}_x \hat{k}_y + \mathbf{B}_{yz} \hat{k}_y \hat{k}_z + \mathbf{B}_{zx} \hat{k}_x \hat{k}_z + \mathbf{C}_x \hat{k}_x + \mathbf{C}_y \hat{k}_y + \mathbf{C}_z \hat{k}_z + V_P, \quad (2)$$

where \mathbf{E}_{bo} is the matrix for the band offsets, \mathbf{A} s, \mathbf{B} s, and \mathbf{C} s are the coefficient matrices.¹² By using the deformation potential theory, an additional part \hat{H}_s ,¹² which has a similar form as $\hat{H}_{\mathbf{k}\cdot\mathbf{p}}$, can be added to take into account the effects of the strain.

Figure 1 plots the energy dispersion of $\text{In}_{0.5}\text{Ga}_{0.5}\text{As}$ bands (dotted lines) calculated by the eight-band $\mathbf{k}\cdot\mathbf{p}$ method. Note a spurious crossing between valence bands at wave vectors k halfway between the Γ and X points. This crossing may result in spurious valence band states in the intermixing SAQDs. The same problem has been reported in the study of InAs dots on InP¹⁷ and can be artificially removed by adding additional terms proportional to k^4 into the eight-band $\mathbf{k}\cdot\mathbf{p}$ Hamiltonian.

C. Tight-binding single-particle states

By using the same number of basis functions as the eight-band $\mathbf{k}\cdot\mathbf{p}$ method, EBOM is a sp^3 tight-binding method

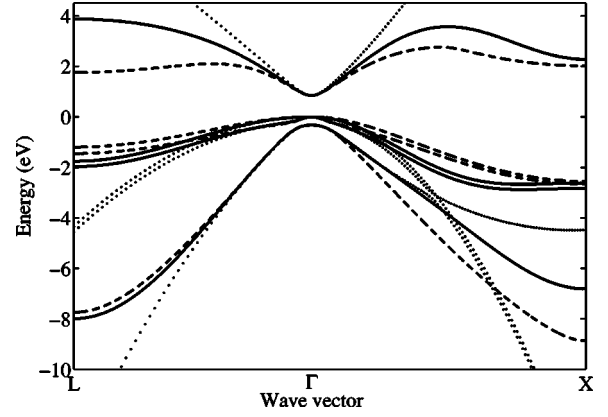


FIG. 1. Band structure of $\text{In}_{0.5}\text{Ga}_{0.5}\text{As}$ described by the eight-band $\mathbf{k}\cdot\mathbf{p}$ method (dotted lines), the tight-bindinglike effective bond-orbital method (solid lines), and the empirical sp^3s^* tight-binding method (dashed lines).

based on an effective fcc lattice,²² i.e., a pair of cation and anion in a zinc blende lattice is treated as a single superatom. The Hamiltonian is given by

$$\langle \mathbf{R}\alpha | \hat{H}_{EB} | \mathbf{R}'\alpha' \rangle = (E_p + V_P) \delta_{\mathbf{R}\mathbf{R}'} \delta_{\alpha\alpha'} + \sum_{\tau} \delta_{\mathbf{R}-\mathbf{R}',\tau} \{ E_{xy} \tau_{\alpha} \tau_{\alpha'} (1 - \delta_{\alpha\alpha'}) + [E_{xx} \tau_{\alpha}^2 + E_{zz} (1 - \tau_{\alpha}^2)] \delta_{\alpha\alpha'} \},$$

$$\langle \mathbf{R}s | \hat{H}_{EB} | \mathbf{R}'s' \rangle = (E_s + V_P) \delta_{\mathbf{R}\mathbf{R}'} + \sum_{\tau} E_{ss} \delta_{\mathbf{R}-\mathbf{R}',\tau},$$

$$\langle \mathbf{R}s | \hat{H}_{EB} | \mathbf{R}'\alpha \rangle = \sum_{\tau} E_{sp} \tau_{\alpha} \delta_{\mathbf{R}-\mathbf{R}',\tau}, \quad (3)$$

where $|\mathbf{R}\alpha\rangle$ denotes an orbital α located at site \mathbf{R} . E_s , E_p , E_{ss} , E_{sp} , E_{xy} , E_{xx} , and E_{zz} are parameters that are chosen to reproduce the conduction-band effective mass, band gap, spin-split energy, and Luttinger parameters.

Figure 1 plots the energy dispersion of $\text{In}_{0.5}\text{Ga}_{0.5}\text{As}$ bands (solid lines) calculated by EBOM. As EBOM uses the same Luttinger parameters as the $\mathbf{k}\cdot\mathbf{p}$ theory does, both approaches give the same band structure near the Γ point. However, the spurious crossing from the eight-band $\mathbf{k}\cdot\mathbf{p}$ theory is not found in the EBOMs band structure. Here, we adopted the parametrization by Loehr.²⁴ For comparison, the band structure of $\text{In}_{0.5}\text{Ga}_{0.5}\text{As}$ by the empirical sp^3s^* tight-binding method (ETBM)^{19,20} is also plotted (dash lines). It is noted that the discrepancy between EBOM and ETBM is much smaller than that between the eight-band $\mathbf{k}\cdot\mathbf{p}$ and ETBM.

Compared with the single-band calculation, the multiband methods gives more realistic confined states in SAQDs. These states lack the symmetries, such as angular momentum and spin, which are usually preserved in the single-band calculation. These symmetries are important in the CI calculation because they substantially reduce the total number of configurations. For disklike or lens-shape dots, the circular symmetry would be broken due to the effects of shear strain. In addition, the total spin S and its projection S_z are not

conserved due to the spin-orbit interaction. However, we will show that the multiband single-particle states are polarized and the polarization can be used to define quasispin.

III. FORMULATION OF THE MULTIEXCITON PROBLEM

Our structure contains millions of atoms and, hence, millions of electrons. As long as the total system contains an energy gap and a well defined ground state wave function, the intractable million electron problem can be replaced by a much smaller problem of pairs of excitations in the form of quasielectrons and quasiholes. Formally, any electron state can be expanded in terms of increasing number of pairs of excitations

$$\Psi = \Psi_0 + \sum_{i,m} c_i^m \Psi_i^m + \sum_{ij,mn} c_{ij}^{mn} \Psi_{ij}^{mn} + \dots, \quad (4)$$

where Ψ_0 is the Hartree-Fock ground state with all valence states occupied and conduction band empty. Ψ_i^m is an excited state formed by removing an electron from the state i in the valence band and creating a ‘‘hole,’’ and moving it to the state m in the conduction band, creating an ‘‘electron.’’ Ψ_{ij}^{mn} is a doubly excited state containing two electrons and two holes, and so on. The number of electron-hole pairs is in principle not conserved and this expansion can be used to describe all excited states.⁴² However, in semiconductors, the difference between the kinetic energies of different numbers of pair excitations is proportional to the band gap, which is much larger than the Coulomb interaction mixing them. Therefore, different numbers of pair excitations are practically independent from each other.^{43–46}

After solving the one electron problem [Eqs. (1)–(3)] and obtaining the single-particle eigenstates ϕ_i and their energies E_i , the Hamiltonian for the interacting electrons can be written in second quantization as

$$\hat{H} = \sum_i E_i c_i^\dagger c_i + \frac{1}{2} \sum_{ijkl} V_{ijkl} c_i^\dagger c_j^\dagger c_k c_l. \quad (5)$$

Here V_{ijkl} 's are the Coulomb matrix elements

$$V_{ijkl} = \iint \phi_i^*(\mathbf{r}_1) \phi_j^*(\mathbf{r}_2) \frac{e^2}{4\pi\epsilon(\mathbf{r}_1, \mathbf{r}_2) \cdot |\mathbf{r}_1 - \mathbf{r}_2|} \cdot \phi_k(\mathbf{r}_2) \times \phi_l(\mathbf{r}_1) d\mathbf{r}_1 d\mathbf{r}_2, \quad (6)$$

$\epsilon(\mathbf{r}_1, \mathbf{r}_2)$ is the dielectric function.³⁶ We replace it with the dielectric constant ϵ throughout the calculation. The method for computation of these elements is given in the Appendix. The Hamiltonian for many-exciton complex can be written as^{32,41}

$$H_{ex} = \sum_i E_i^e c_i^\dagger c_i - \sum_i E_i^h h_i^\dagger h_i - \sum_{ijkl} V_{ijkl}^{he} h_i^\dagger c_j^\dagger c_k h_l + \sum_{ijkl} X_{ijkl} h_i^\dagger c_j^\dagger c_k h_l + \frac{1}{2} \sum_{ijkl} V_{ijkl}^{ee} c_i^\dagger c_j^\dagger c_k c_l + \frac{1}{2} \sum_{ijkl} V_{ijkl}^{hh} h_i^\dagger h_j^\dagger h_k h_l. \quad (7)$$

The electron-hole exchange interaction elements, X_{ijkl} are defined by

$$X_{ijkl} = \iint \phi_i^*(\mathbf{r}_1) \phi_j^*(\mathbf{r}_2) \frac{e^2}{4\pi\epsilon(\mathbf{r}_1, \mathbf{r}_2) \cdot |\mathbf{r}_1 - \mathbf{r}_2|} \cdot \phi_k(\mathbf{r}_1) \times \phi_l(\mathbf{r}_2) d\mathbf{r}_1 d\mathbf{r}_2. \quad (8)$$

IV. EXCITON RECOMBINATION

In order to calculate the photoluminescence spectrum, one needs to calculate eigenstates of both N exciton and $N-1$ exciton systems. At low temperature, only the ground state and a few excited states of the N exciton system are required. However, in order to obtain the spectrum over a broad energy range, a larger number of eigenstates of the $N-1$ exciton system has to be calculated. In general, about 1000–2000 eigenstates of the $N-1$ exciton system are required to cover transitions occurring in the s and p shells.

Let us begin with recombination of noninteracting electrons. The momentum matrix element between an electron state $\phi_e = \sum_n \psi_n^e u_n$ and a hole state $\phi_h = \sum_n \psi_n^h u_n$ is given by

$$\langle \phi_h | \mathbf{e} \cdot \hat{\mathbf{p}} | \phi_e \rangle = \sum_{mn} \langle u_n | \mathbf{e} \cdot \hat{\mathbf{p}} | u_m \rangle \langle \psi_n^h | \psi_m^e \rangle + \sum_m \langle \psi_m^h | \mathbf{e} \cdot \hat{\mathbf{p}} | \psi_m^e \rangle. \quad (9)$$

Here, ψ_n 's are the envelop functions and the basis functions u_n 's are chosen as eight uncoupled spin-orbitals, i.e., $|s \uparrow\rangle$, $|x \uparrow\rangle$, $|y \uparrow\rangle$, $|z \uparrow\rangle$, $|s \downarrow\rangle$, $|x \downarrow\rangle$, $|y \downarrow\rangle$, and $|z \downarrow\rangle$. If we neglect the contribution from the envelope-function part of the wave function $\sum_m \langle \psi_m^h | \mathbf{e} \cdot \hat{\mathbf{p}} | \psi_m^e \rangle$,¹³ it can be further simplified as

$$\begin{aligned} \langle \phi_h | \hat{p}_x | \phi_e \rangle &= iP_0 \cdot [\langle \psi_{x\uparrow}^h | \psi_{s\uparrow}^e \rangle + \langle \psi_{x\downarrow}^h | \psi_{s\downarrow}^e \rangle] - \langle \psi_{s\uparrow}^h | \psi_{x\uparrow}^e \rangle \\ &\quad - \langle \psi_{s\downarrow}^h | \psi_{x\downarrow}^e \rangle, \\ \langle \phi_h | \hat{p}_y | \phi_e \rangle &= iP_0 \cdot [\langle \psi_{y\uparrow}^h | \psi_{s\uparrow}^e \rangle + \langle \psi_{y\downarrow}^h | \psi_{s\downarrow}^e \rangle] - \langle \psi_{s\uparrow}^h | \psi_{y\uparrow}^e \rangle \\ &\quad - \langle \psi_{s\downarrow}^h | \psi_{y\downarrow}^e \rangle, \end{aligned} \quad (10)$$

where $iP_0 = \langle s | \hat{p}_x | x \rangle = \langle s | \hat{p}_y | y \rangle$ denotes the coupling between the conduction and valence bands. For circular polarization σ^+ or σ^- , the momentum matrix element is then given by $P_{he}^\pm = 1/\sqrt{2}(\langle \phi_h | \hat{p}_x | \phi_e \rangle \mp i \langle \phi_h | \hat{p}_y | \phi_e \rangle)$.

In the single-band effective-mass method, the Bloch functions for the heavy hole are $u_{h\uparrow} = 1/\sqrt{2}(|x \uparrow\rangle + i|y \uparrow\rangle)$ for $j_z = 3/2$ and $u_{h\downarrow} = 1/\sqrt{2}(|x \downarrow\rangle - i|y \downarrow\rangle)$ for $j_z = -3/2$. Hence, we have $P_{he}^- = \langle \phi_{h\uparrow} | \hat{p}^- | \phi_{e\uparrow} \rangle = \langle u_{h\uparrow} | 1/\sqrt{2}(\hat{p}_x + i\hat{p}_y) | s \uparrow \rangle \langle \psi_h | \psi_e \rangle = -iP_0 \langle \psi_h | \psi_e \rangle$. It is straightforward to show that $P_{he}^- = P_{he}^+$.

The intensity of photoluminescence from the recombination of one electron-hole pair in a N -exciton state is defined as^{34,41}

$$I_{\sigma_\pm}(h\nu) = \sum_i f(E_N^i) \sum_f |\langle C_{N-1}^f | P_{\sigma_\pm}^- | C_N^i \rangle|^2 \cdot \delta(E_N^i - E_{N-1}^f - h\nu), \quad (11)$$

where C_N^i is the i th eigenstate of the N -exciton system. Note that $\langle C_{N-1}^f | P_{\sigma_\pm}^- | C_N^i \rangle$ coherently sums all the possible recombi-

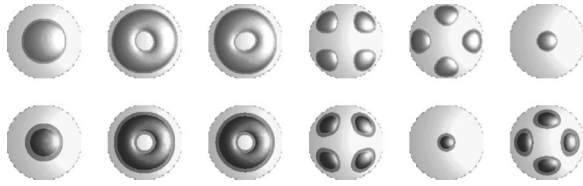


FIG. 2. Two-dimensional plot of the density of first six electron (first row) and hole (second row) wave functions calculated by the multiband $\mathbf{k}\cdot\mathbf{p}$ method.

nations, therefore, the interference effect may play an important role.

The probability function is defined as $f(E_N^i) = \exp(-E_N^i/\kappa T) / \sum_j \exp(-E_N^j/\kappa T)$. The operator $P_{\sigma_{\pm}}^-$ describes all the possible electron-hole recombination, namely

$$P_{\sigma_{\pm}}^- = \sum_{nm} p_{nm}^{\pm} h_n c_m. \quad (12)$$

In the absence of magnetic field, we have $I_{\sigma_+}(E) = I_{\sigma_-}(E)$.

V. RESULTS AND DISCUSSION

We now illustrate our method by a calculation for a model structure of $\text{In}_{0.5}\text{Ga}_{0.5}\text{As}/\text{GaAs}$ disklike SAQD characteristic of SAQDs grown using In-flush method.⁴⁷ The dot has diameter 25.4 nm along the base and 2.3 nm height along the growth direction and has a wetting layer of 0.6 nm. The composition and dimensions of the dot are chosen such that its emission spectrum is similar to the one observed in the experiment of Raymond *et al.*⁴⁸ We also adopt the virtual crystal approximation in order to compare results from different models. The strain distribution is calculated by the continuum elasticity theory^{18,49} on a large cubic finite-difference mesh that has 120 nm along each dimension and Dirichlet boundary condition on each side in order to ensure that the strain is fully relaxed.

In Fig. 2, we show the probability density of the first six electron (in the upper row) and six hole states (lower row) calculated by the multiband $\mathbf{k}\cdot\mathbf{p}$ method. The corresponding energy levels are plotted in Fig. 3. The material parameters used in the calculation are taken from Ref. 14.

The circular symmetry of the single-particle states is found basically preserved due to the small shear strain and weak piezoelectric potential in this intermixing quantum dot. Hence, the states in the conduction band and valence bands are seen to group into three shell, respectively. In the second shell, the shear strain induces a small splitting of 1.3 meV between the two p -like valence-band states. In the third shell, the splitting is about 3 meV and the disklike geometry is responsible for the splitting between the two $3d$ states and the $2s$ state. It should also be noted that the ordering of the electron states in this shell is different from that of the hole states.

In the single-band effective mass calculation, the four effective mass parameters are chosen to fit the ground state energies and the separations between the ground states and first excited states that are obtained by the $\mathbf{k}\cdot\mathbf{p}$ method, which gives (in unit of free electron mass m_0) $m_{\parallel}^e = 0.060$,

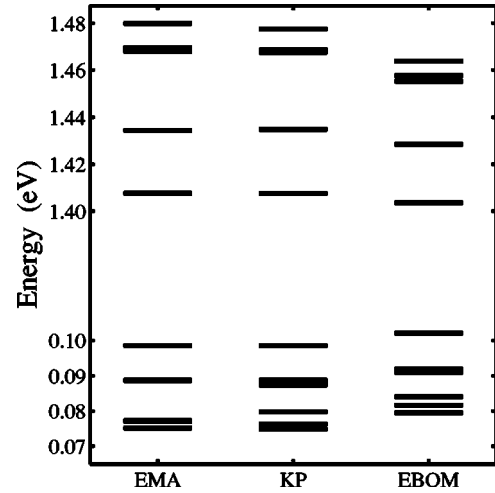


FIG. 3. Calculated energy levels of the $\text{In}_{0.5}\text{Ga}_{0.5}\text{As}/\text{GaAs}$ self-assembled quantum dot by the eight-band $\mathbf{k}\cdot\mathbf{p}$ (KP) method and EBOM. Also shown are the energy levels fitted for the effective-mass approximation (EMA).

$m_{\perp}^e = 0.070$, $m_{\parallel}^h = 0.27$, and $m_{\perp}^h = 0.30$. It is noted that the electron effective mass in the dot is larger than the bulk value 0.045 for $\text{In}_{0.5}\text{Ga}_{0.5}\text{As}$ and approaches the value in bulk GaAs. Compared with those in bulk InAs, the holes in the dot are much lighter in the plane perpendicular to the growth direction. Similar findings that the effective mass of electrons in quantum dots exceeds the value in the corresponding bulk dot material and approach that in the bulk matrix material and the in-plane component of the effective mass of holes becomes much lighter have been reported.^{5,50}

In valence bands, the heavy hole and light hole are decoupled by the biaxial strain. For dots of small height, the biaxial strain is almost constant inside the structure, hence, the low-lying states in valence bands are mostly heavy-hole states. This is the reason why these states can be fitted by using single-band approximation. For thick dots, the band edges of heavy hole and light hole may cross each other due to the fact that the biaxial strain changes its sign inside the structure, which results in more light-hole components in the hole states in these dots.

The energy levels calculated by EBOM differs from those by the $\mathbf{k}\cdot\mathbf{p}$ method, especially for the high-lying states. The shell separations by EBOM are smaller than those by the $\mathbf{k}\cdot\mathbf{p}$ method. For example, in the conduction band, E_{s-p} (separation between s and p shell) is 24.8 meV by EBOM and 27.3 meV by the $\mathbf{k}\cdot\mathbf{p}$ method, respectively. The averaged separations E_{p-d} between different models are even larger, 30.6 meV from EBOM and 36.4 meV from the $\mathbf{k}\cdot\mathbf{p}$ method.

As shown in Fig. 1, the band structure predicted by the eight-band $\mathbf{k}\cdot\mathbf{p}$ method and EBOM match only in the region close to the Γ point. Although the lateral dimensions of the quantum-dot structure are large, it is small (2.3 nm) along the growth direction. Hence, the confined electron and hole states include components with large k_z , which results in different energies for these states. For dots with larger height, there is very little discrepancy found between the two methods.²³

A. Polarization of single-particle states

In the framework of the envelope function formalism, it is possible to separate the components of an envelope function into two groups when the spin-orbit interaction is not very strong. One group consists of components for spin up basis functions, $|s \uparrow\rangle$, $|x \uparrow\rangle$, $|y \uparrow\rangle$, and $|z \uparrow\rangle$, and the other consists of components for spin down basis functions. We define polarization of state ϕ as

$$p = \int |\psi_{s\uparrow}(\mathbf{r})|^2 + |\psi_{x\uparrow}(\mathbf{r})|^2 + |\psi_{y\uparrow}(\mathbf{r})|^2 + |\psi_{z\uparrow}(\mathbf{r})|^2 d\mathbf{r}. \quad (13)$$

A state is polarized if either $p \approx 1$ (a “spin” up state) or $p \approx 0$ (a spin down state). Apparently, there is little overlap between the polarized states with different polarization.

A careful examination of the calculated single-particle states shows that all the single-particle states in the conduction band consist of less than 1% component from the split-off band while for valence band states it is less than 5%. Hence, the mixture between spin up and spin down components in any of these states should be very small, i.e., they are polarized.

However, in the absence of magnetic fields, all the single-particle states calculated by the $\mathbf{k}\cdot\mathbf{p}$ method and EBOM are doubly degenerate due to the time-reversal symmetry.¹⁶ Instead of having two degenerate states, the numerical calculation can only give one state from a random linear combination of the two polarized and degenerate states. Because of this degeneracy, most of the calculated single-particle states are found not polarized. By applying a small magnetic field (1 mT) along the growth direction, this time-reversal symmetry can be removed and polarized single-particle states are recovered. The eight-band $\mathbf{k}\cdot\mathbf{p}$ Hamiltonian is modified⁵¹ to include the effects of magnetic fields. For EBOM, we introduce Peierls phase factor⁵² to include the magnetic field in the Hamiltonian.

B. Electron-hole exchange interaction

The ground state of a single exciton is a dark doublet separated from a bright doublet by the exchange energy. A dark (bright) exciton state is dominated by a configuration of an electron and a hole in their respective ground state with the opposite (same) spin. The bright doublet has a higher energy due to the electron-hole exchange energy. Because of the relatively large size of SAQDs, the electron-hole exchange interaction causes a very small correction to exciton states. It can be measured from the fine structure of single exciton recombination spectrum.⁵³

An accurate calculation of the electron-hole exchange will require knowledge of both electron and hole states and the dielectric function at a microscopic level.^{36,37} However, for SAQDs, the exchange energy can be estimated by using the multiband $\mathbf{k}\cdot\mathbf{p}$ theory or EBOM, where the electron-hole exchange interaction arises from the mixing between the conduction and valence bands. The calculation for our structure shows that the separation between the dark and bright doublets of a single exciton is $74.6 \mu\text{eV}$, which includes an

electron-hole exchange energy $63.2 \mu\text{eV}$ and the correlation effect. It gives a fairly good agreement with the value derived from the experiment⁵³ on similar samples, considering the approximation made in the theory, and the uncertainty in the dot size, shape, and composition in the experiment. Because of the small contribution of the electron-hole exchange interaction, we neglect it in the subsequent calculation.

C. Addition energies and hidden symmetry in multiexciton complexes

Due to the presence of quasishell structure in the single-particle energy spectrum, we chose the first 12 electron and 12 hole states (with quasispins), which form the first three shells in conduction and valence bands, respectively, to build the multiexciton configurations.

In order to reduce the total number of configurations which grows factorially with the size of single-particle basis set, we impose an additional constraint on the exciton configurations, i.e., the sum of the electron quasispins should be equal to that of the hole quasispins.⁴¹ We also apply a truncation according to the Hartree-Fock energies of configurations in order to limit the total number of the configurations to less than 50 000.

Hidden symmetry^{8,33,34,41} is a good approximation in a multiexciton system with degenerate single-particle states and symmetric electron-electron, electron-hole, and hole-hole interactions. It predicts that the chemical potential, i.e., the energy required to add an electron-hole pair to the system, is independent of the number of excitons within a degenerate shell.

The symmetry between electron-electron, electron-hole, and hole-hole interactions is broken because the hole states are usually more confined than the electrons in the conduction bands. Hence, the hole-hole interaction is generally stronger than the electron-electron interaction. The calculation by the multiband $\mathbf{k}\cdot\mathbf{p}$ (single-band effective-mass) method shows $V_{1111}^{ee} = 14.4(14.9) \text{ meV}$, $V_{1111}^{hh} = 16.7(19.4) \text{ meV}$, and $V_{1111}^{he} = 15.4(16.6) \text{ meV}$. The EBOM gives similar values, which are 13.9, 16.3, and 14.9 meV, respectively. In the case of either $\mathbf{k}\cdot\mathbf{p}$ or EBOM, the hole-hole interaction is stronger than the electron-electron interaction by about 15%. The hole states from the single-band calculation are found more confined than those from the two multiband calculations.

Figure 4 plots the calculated addition energies for different number of excitons. Both the $\mathbf{k}\cdot\mathbf{p}$ method and EBOM give similar result except that the EBOM predicts lower values. The result of the single-band effective-mass approximation is found very close to that by the $\mathbf{k}\cdot\mathbf{p}$ method. A clear plateau structure can be found associated with the shell structure, which is an apparent signature of hidden symmetry. The fluctuation in the addition energies within the same shell is not larger than that in the single-particle energies or the difference among the electron (hole)-electron (hole) interactions. The $\mathbf{k}\cdot\mathbf{p}$ method gives the largest fluctuation, 1.4 meV in the p shell and 4.5 meV in the d shell, while EBOM gives 1.7 and 2.7 meV, respectively. It is therefore seen that the hidden symmetry in our structure is well preserved, and not

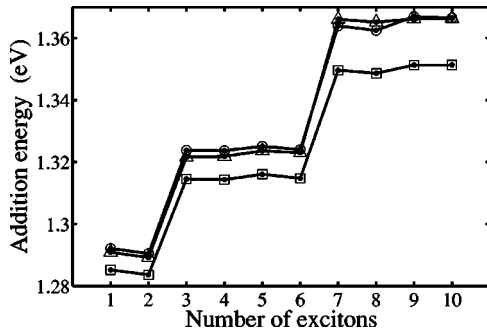


FIG. 4. Addition energy spectra $\mu(N)=E_g(N)-E_g(N-1)$, calculated by the single-band effective-mass approximation (triangular dots), the multiband $\mathbf{k}\cdot\mathbf{p}$ method (circular dots) and EBOM (square dots) for the $\text{In}_{0.5}\text{Ga}_{0.5}\text{As}/\text{GaAs}$ disklike quantum dot.

sensitive either to the splitting of p and d shells or the asymmetric interactions.

D. Emission spectra

Figures 5, 6, and 7 show the emission spectra calculated by the single-band effective-mass method, the eight-band $\mathbf{k}\cdot\mathbf{p}$ method, and EBOM, respectively, for up to six excitons. As the $\mathbf{k}\cdot\mathbf{p}$ method and EBOM are shown to give very similar results except for overall shifts in transition energies, we will confine our attention to analyzing the difference between the results by the single-band and the multiband $\mathbf{k}\cdot\mathbf{p}$ calculations. It should be mentioned that the spectra in Figs. 5 and 6 are plotted in different scale, only the relative intensity between the spectra in the same figure is relevant.

The difference between the single-band and multiband calculations concentrates in the s shell as the emission peaks in the p shell are found similar between Figs. 5 and 6. Compared with the single-band calculation, the band-mixing effect enables more configurations from the multiband single-

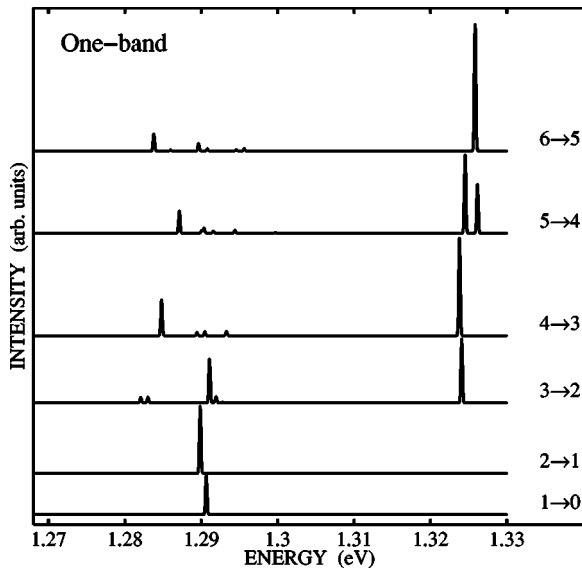


FIG. 5. Excitonic emission spectra calculated by the single-band effective-mass method.

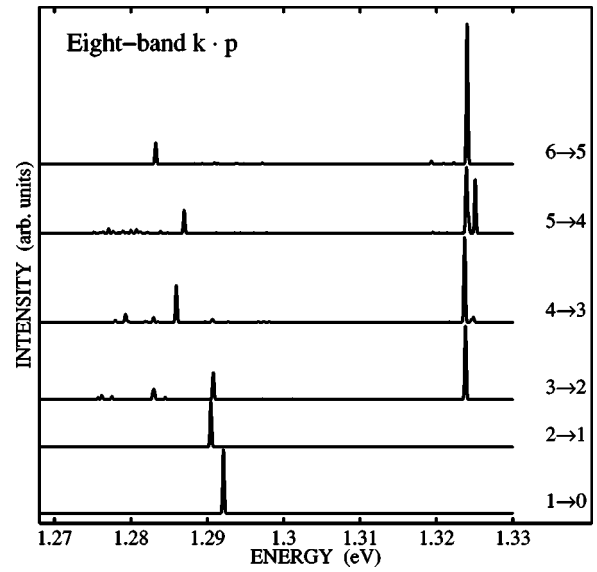


FIG. 6. Excitonic emission spectra calculated by the multiband $\mathbf{k}\cdot\mathbf{p}$ method.

particle states to be coupled through the Coulomb interaction. It results in more possible yet weak transitions in the low energy end of the spectra, as are found in Figs. 6 and 7 when the number of excitons is larger than 4.

This is illustrated in Fig. 8. In the emission spectra from the three-exciton complex (3X), all the three methods give one strong peak in the p -shell region and exhibit different structure in the s -shell region. The single-band calculation gives one peak with high intensity and three other small peaks in the s -shell region while both the $\mathbf{k}\cdot\mathbf{p}$ method and EBOM show five peaks with visible intensities.

The initial state of the recombination from 3X is its ground state and the final states associated with peaks found in the s -shell region are excited biexciton states.³⁴ As there is little difference among the 3X ground states calculated by different methods, it is the excited biexciton states that ac-

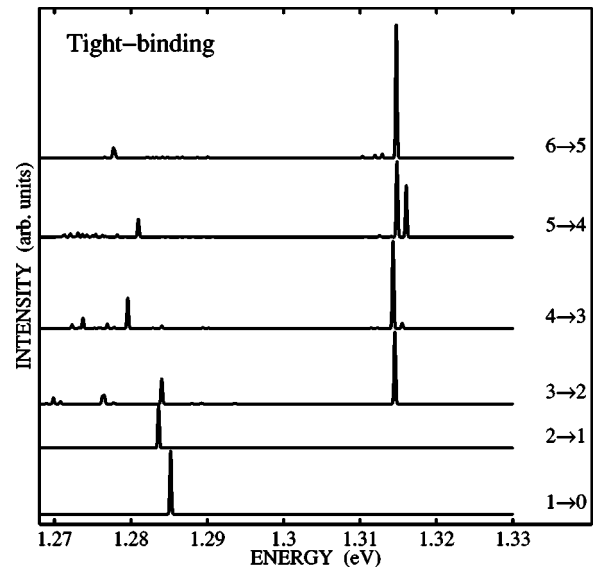


FIG. 7. Excitonic emission spectra calculated by EBOM.

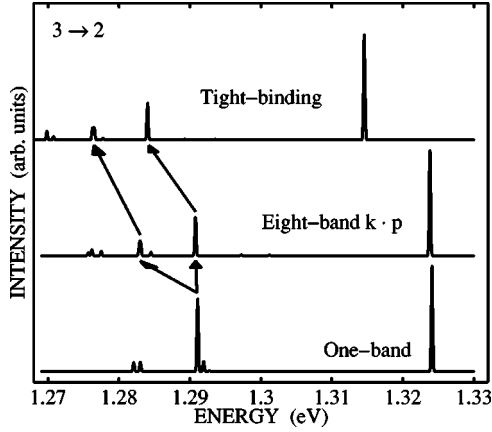


FIG. 8. Emission spectra from three-exciton complex calculated by different methods.

count for the different structure in the emission spectra.

In the single-band calculation, the emission peak with high intensity in the s -shell region is associated with three biexciton states where both the two electrons and the two holes are in a triplet configuration (one in the s shell and the other in the p shell). In these states, the total spin $S(=1)$ and its z -component S_z of the two electrons are the same as those of the two holes. As the spin-orbit interaction is absent in the single-band calculation, these three biexciton states of different S_z are degenerate and give rise to only one peak in the s -shell region.

In the presence of spin-orbit interaction which is taken into account in both the $\mathbf{k} \cdot \mathbf{p}$ method and EBOM, the degeneracy among these three biexciton states is partially lifted, i.e., the biexciton state of $|S_z|=1$ has a different energy from that of $S_z=0$. It gives rise to two splitted peaks in the s -shell region, as illustrated in Fig. 8. The three other smaller peaks are associated with those excited biexciton states in singlet-singlet or singlet-triplet configurations, which are less affected by the spin-orbit interaction, and can be seen in the all spectra.

VI. CONCLUSIONS

In conclusion, we have presented a multiband microscopic theory of many-exciton complexes in self-assembled quantum dots. Three methods: single-band effective-mass approximation, the multiband $\mathbf{k} \cdot \mathbf{p}$ method, and the tight-binding-like EBOM, are used to obtain single-particle states. We expand the many-body wave functions of N electrons and N valence holes in the basis of Slater determinants. The Coulomb matrix elements are evaluated using statically screened interaction and the correlated N -exciton states are obtained by the configuration interaction method. We apply the theory to the excitonic emission spectrum in InAs/GaAs self-assembled quantum dots and successfully compare the results of the single-band effective-mass approximation with those obtained by using the of $\mathbf{k} \cdot \mathbf{p}$ and tight-binding methods.

ACKNOWLEDGMENTS

This work is supported by the NRC HPC project, NRC-HELMHOLTZ grant, and CIAR. The authors would like to

thank M. Korkusiński, S. Patchkovskii, and J. Tse for discussions.

APPENDIX A: COULOMB MATRIX ELEMENTS

In this appendix, we describe an efficient approach to calculate Coulomb matrix elements numerically. In the configuration interaction method, the properties of the system are given by the single particle spectrum and by the Coulomb matrix elements defined as two-electron integrals [see Eq. (6)]. One possible way to calculate these six-dimensional integrals is to first solve Poisson equation, then calculate reduced three-dimensional integrals.⁵⁴ The calculation is repeated for each integrals. For the calculation involving 12 electron states and 12 hole states, the total number of integrals is almost 10 000. Here we propose an algorithm that does not require calculation for each integrals.

Within the envelope function formalism, the wave functions of single-particle states are expressed as a linear combination of Bloch sums

$$\phi_i(\mathbf{r}) = \frac{1}{\sqrt{N}} \sum_n \sum_{\mathbf{R}} \psi_{in}(\mathbf{R}) u_n(\mathbf{r} - \mathbf{R}), \quad (\text{A1})$$

where ψ_{in} is the n th component of the envelop function ψ_i , $u_n(\mathbf{r} - \mathbf{R})$ is the n th atomic orbital localized at unit cell \mathbf{R} and $1/\sqrt{N} \sum_n u_n(\mathbf{r} - \mathbf{R})$ is the corresponding Bloch function. If we ignore the contribution from these localized atomic orbitals and replace $\mathbf{r}_1 - \mathbf{r}_2$ with $\mathbf{R}_1 - \mathbf{R}_2$ in Eq. (6), we have

$$V_{ijkl} = \sum_{\mathbf{R}_1, \mathbf{R}_2} \sum_m \psi_{im}^*(\mathbf{R}_1) \psi_{lm}(\mathbf{R}_1) \cdot \frac{e^2}{4\pi\epsilon \cdot |\mathbf{R}_1 - \mathbf{R}_2|} \times \sum_n \psi_{jn}^*(\mathbf{R}_2) \psi_{kn}(\mathbf{R}_2). \quad (\text{A2})$$

We further transform a three-dimensional (3D) wave function $\psi(\mathbf{R})$ into a column vector $\psi(r)$ by mapping the 3D variable \mathbf{R} onto a one-dimensional index r , a six-dimensional integral can be converted into a vector-matrix multiplication

$$V_{ijkl} = \left(\sum_m \psi_{im}^* \otimes \psi_{lm} \right)^T \cdot U \cdot \left(\sum_n \psi_{jn}^* \otimes \psi_{kn} \right), \quad (\text{A3})$$

where \otimes is the direct multiplication (element by element) operator between two vectors. U is the matrix with elements $U(r_1, r_2) = e^2 / (4\pi\epsilon \cdot |\mathbf{R}_1 - \mathbf{R}_2|)$. The diagonal elements can be obtained by the integration of $1/R$ over a unit cell.

In order to use the optimized Basic Linear Algebra Subprograms (BLAS) library,⁵⁵ the above formulation can be further vectorized as

$$J = \Phi^T \cdot U \cdot \Phi, \quad (\text{A4})$$

where $\Phi_{r,\{ij\}} = \sum_n \psi_{in}^*(r) \psi_{jn}(r)$ is a matrix containing all the possible pairs of two-particle wave functions. Due to the large dimension of matrix U , we make use of domain decomposition in the numerical calculation to divide it into a number of smaller matrices and sum up the result of all the individual multiplications.

APPENDIX B: COMPANION CONFIGURATION AND ADDITIVITY RULE

In this Appendix, we point out how to use the additivity rule to construct configurations for multiexcitons. As a multiexciton complex contains two different particles, electrons and holes, the total number of possible configurations is much larger than for electrons or holes separately. To circumvent this difficulty, we use the following algorithm for construction of multiexciton configurations.

The many-body Hamiltonian matrix constructed from the CI method is a sparse matrix. For a given configuration, there is only a small number of configurations interacting with it, which are named as its *companion* configurations. Let us first define the distance between configuration C_i and C_j , $\|C_i, C_j\|$, as the total number of single-particle states that the two configurations differ by. It is apparent that

$$\langle C_i | \hat{H} | C_j \rangle = 0, \quad \text{if } \|C_i, C_j\| > 2. \quad (\text{B1})$$

An exciton configuration consists of a part for electron(s) and the other part for hole(s), i.e., $C_i^{ex} = \{C_i^e, C_i^h\}$. The distance between two exciton configurations, C_i^{ex} and C_j^{ex} , can be easily calculated by the *additivity* rule, namely

$$D_{ij}^{ex} = \|C_i^{ex}, C_j^{ex}\| = \|C_i^e, C_j^e\| + \|C_i^h, C_j^h\| = D_{ij}^e + D_{ij}^h. \quad (\text{B2})$$

One can calculate the distance matrix D_e and D_h for the electron and hole configurations, respectively, and then obtain the matrix D_{ex} by using the additivity rule. When the number of single particle states (either electrons or holes) is large, a cutoff is necessary to be applied to the total number of electron or hole configurations. Depending on the memory available for the computation, it is set to be between 5000 and 10 000. Once the distance matrix D_{ex} for the exciton configurations is calculated, it is straightforward to construct the configuration interaction matrix as the positions of all the non-zero matrix elements are known.

*Electronic address: weidong.sheng@nrc-cnrc.gc.ca

†Present address: Electrophysics Department, National Chiao Tung University, Hsinchu 30050, Taiwan, Republic of China.

¹L. Jacak, P. Hawrylak, and A. Wojs, *Quantum Dots* (Springer, Berlin, 1998).

²D. Bimberg, M. Grundmann, and N. N. Ledentsov, *Quantum Dot Heterostructures* (Wiley, New York, 1998).

³P. Hawrylak and M. Korkusinski, *Electronic Properties of Self-Assembled Quantum Dots*, in *Single Quantum Dots*, edited by P. Michler (Springer, Berlin, 2003).

⁴G. W. Bryant, Phys. Rev. B **37**, 8763 (1988); Y. Z. Hu *et al.*, *ibid.* **42**, 1713 (1990); V. Halonen *et al.*, *ibid.* **45**, 5980 (1992); W. Que, *ibid.* **45**, 11036 (1992); U. Bockelmann, *ibid.* **48**, 17 637 (1993); S. V. Nair and T. Takagahara, *ibid.* **55**, 5153 (1997); A. Franceschetti and A. Zunger, Phys. Rev. Lett. **78**, 915 (1997).

⁵H. Drexler, D. Leonard, W. Hansen, J. P. Kotthaus, and P. M. Petroff, Phys. Rev. Lett. **73**, 2252 (1994).

⁶M. J. Steer, D. J. Mowbray, W. R. Tribe, M. S. Skolnick, M. D. Sturge, M. Hopkinson, A. G. Cullis, C. R. Whitehouse, and R. Murray, Phys. Rev. B **54**, 17 738 (1996).

⁷R. Cingolani, R. Rinaldi, H. Lipsanen, M. Sopanen, R. Virkkala, K. Majjala, J. Tulkki, J. Ahopelto, K. Uchida, N. Miura, and Y. Arakawa, Phys. Rev. Lett. **83**, 4832 (1999).

⁸M. Bayer, O. Stern, P. Hawrylak, S. Fafard, and A. Forchel, Nature (London) **405**, 923 (2000).

⁹A. Hartmann, Y. Ducommun, E. Kapon, U. Hohenester, and E. Molinari, Phys. Rev. Lett. **84**, 5648 (2000).

¹⁰P. Hawrylak, G. A. Narvaez, M. Bayer, and A. Forchel, Phys. Rev. Lett. **85**, 389 (2000).

¹¹K. Karrai, R. J. Warburton, C. Schulhauser, A. Högele, B. Urbaszek, E. J. McGhee, A. O. Govorov, J. M. Garcia, B. D. Gerardot, and P. M. Petroff, Nature (London) **427**, 138 (2004).

¹²Thomas B. Bahder, Phys. Rev. B **41**, 11 992 (1990).

¹³H. Jiang and J. Singh, Phys. Rev. B **56**, 4696 (1997); IEEE J. Quantum Electron. **34**, 1188 (1998).

¹⁴Craig Pryor, Phys. Rev. B **57**, 7190 (1998).

¹⁵W. Sheng and J.-P. Leburton, Appl. Phys. Lett. **80**, 2755 (2002).

¹⁶O. Stier, M. Grundmann, and D. Bimberg, Phys. Rev. B **59**, 5688 (1999).

¹⁷M. Holma, M.-E. Pistol, and C. Pryor, J. Appl. Phys. **92**, 932 (2002).

¹⁸M. Tadić, F. M. Peeters, K. L. Janssens, M. Korkusiński, and P. Hawrylak, J. Appl. Phys. **92**, 5819 (2002).

¹⁹S. Lee, L. Jonsson, J. W. Wilkins, G. W. Bryant, and G. Klimeck, Phys. Rev. B **63**, 195318 (2001).

²⁰S. Lee, J. Kim, L. Jönsson, J. W. Wilkins, G. W. Bryant, and G. Klimeck, Phys. Rev. B **66**, 235307 (2002).

²¹A. J. Williamson, L. W. Wang, and Alex Zunger, Phys. Rev. B **62**, 12 963 (2000).

²²Yia-Chung Chang, Phys. Rev. B **37**, 8215 (1988).

²³S. J. Sun and Y.-C. Chang, Phys. Rev. B **62**, 13 631 (2000).

²⁴John P. Loehr, Phys. Rev. B **50**, 5429 (1994).

²⁵A. Zrenner, M. Markmann, A. Paassen, A. L. Efros, M. Bichler, W. Wegscheider, G. Böhm, and G. Abstreiter, Physica B **256**, 300 (1998).

²⁶S. Raymond, P. Hawrylak, C. Gould, S. Fafard, A. Sachrajda, M. Potemski, A. Wojs, S. Charbonneau, D. Leonard, P. M. Petroff, and J. L. Merz, Solid State Commun. **101**, 883 (1997).

²⁷L. Landin, M. S. Miller, M.-E. Pistol, C. E. Pryor, and L. Samuelson, Science **280**, 262 (1998).

²⁸R. Heitz, F. Guffarth, I. Mukhametzhanov, M. Grundmann, A. Madhukar, and D. Bimberg, Phys. Rev. B **62**, 16 881 (2000).

²⁹M. Baier, F. Findeis, A. Zrenner, M. Bichler, and G. Abstreiter, Phys. Rev. B **64**, 195326 (2001).

³⁰D. Dalacu, D. Poitras, J. Lefebvre, P. J. Poole, G. C. Aers, and R. L. Williams, Appl. Phys. Lett. **82**, 4803 (2003).

³¹A. Szabo and N. S. Ostlund, *Modern Quantum Chemistry: Introduction to Advanced Electronic Structure Theory* (McGraw-Hill, New York, 1989).

³²A. Barenco and M. A. Dupertuis, Phys. Rev. B **52**, 2766 (1995).

³³A. Wojs and P. Hawrylak, Solid State Commun. **100**, 487 (1996); P. Hawrylak and A. Wojs, Semicond. Sci. Technol. **11**, 1516 (1996).

³⁴Pawel Hawrylak, Phys. Rev. B **60**, 5597 (1999).

- ³⁵M. Brasken, M. Lindberg, D. Sundholm, and J. Olsen, *Phys. Rev. B* **61**, 7652 (2000).
- ³⁶A. Franceschetti, H. Fu, L. W. Wang, and A. Zunger, *Phys. Rev. B* **60**, 1819 (1999).
- ³⁷G. Bester, S. Nair, and A. Zunger, *Phys. Rev. B* **67**, 161306(R) (2003).
- ³⁸A. Wojs, P. Hawrylak, S. Fafard, and L. Jacak, *Phys. Rev. B* **54**, 5604 (1996).
- ³⁹L. R. C. Fonseca, J. L. Jimenez, J. P. Leburton, and R. M. Martin, *Phys. Rev. B* **57**, 4017 (1998).
- ⁴⁰Marek Korkusiński and Pawel Hawrylak, *Phys. Rev. B* **63**, 195311 (2001).
- ⁴¹S. J. Cheng, W. Sheng, and P. Hawrylak, *Phys. Rev. B* **68**, 235330 (2003).
- ⁴²P. Hawrylak, A. Wojs, and J. A. Brum, *Phys. Rev. B* **54**, 11 397 (1996).
- ⁴³R. S. Knox, *Solid State Phys.* **5**, 25 (1963).
- ⁴⁴H. Haken, *Quantum Field Theory of Solids: An Introduction* (North Holland, Amsterdam, 1976), pp. 151–166.
- ⁴⁵C. D. Sherrill and H. F. Schaefer, in *Advances in Quantum Chemistry*, edited by P.-O. Lowdin (Academic Press, New York, 1999), Vol. 34, pp. 143–269.
- ⁴⁶A. J. Williamson, A. Franceschetti and A. Zunger, *Europhys. Lett.* **53**, 59 (2001).
- ⁴⁷Z. R. Wasilewski, S. Fafard, and J. P. McCaffrey, *J. Cryst. Growth* **201–202**, 1131 (1999).
- ⁴⁸S. Raymond, S. Studenikin, A. Sachrajda, Z. Wasilewski, S. J. Cheng, W. Sheng, P. Hawrylak, A. Babinski, M. Potemski, G. Ortner, and M. Bayer, *Phys. Rev. Lett.* **92**, 187402 (2004).
- ⁴⁹C. Pryor, J. Kim, L. W. Wang, A. J. Williamson, and A. Zunger, *J. Appl. Phys.* **83**, 2548 (1998).
- ⁵⁰C. Schulhauser, D. Haft, R. J. Warburton, K. Karrai, A. O. Govorov, A. V. Kalameitsev, A. Chaplik, W. Schoenfeld, J. M. Garcia, and P. M. Petroff, *Phys. Rev. B* **66**, 193303 (2002).
- ⁵¹L. R. Ram-Mohan, K. H. Yoo, and R. L. Aggarwal, *Phys. Rev. B* **38**, 6151 (1988).
- ⁵²M. Graf and P. Vogl, *Phys. Rev. B* **51**, 4940 (1995).
- ⁵³M. Bayer, G. Ortner, O. Stern, A. Kuther, A. A. Gorbunov, A. Forchel, P. Hawrylak, S. Fafard, K. Hinzer, T. L. Reinecke, S. N. Walck, J. P. Reithmaier, F. Klopff, and F. Schafer, *Phys. Rev. B* **65**, 195315 (2002).
- ⁵⁴R. Heitz, O. Stier, I. Mukhametzhanov, A. Madhukar, and D. Bimberg, *Phys. Rev. B* **62**, 11 017 (2000).
- ⁵⁵See <http://www.netlib.org/blas/>, for details.